REACTOR DOSIMETRY APPLICATIONS USING RAPTOR-M3G: A NEW PARALLEL 3-D RADIATION TRANSPORT CODE

GIANLUCA LONGONI

Radiation Engineering & Analysis Group,
Westinghouse Electric Co. LLC, Madison, PA 15663, USA

STANWOOD L. ANDERSON

Radiation Engineering & Analysis Group,
Westinghouse Electric Co. LLC, Madison, PA 15663, USA

The numerical solution of the Linearized Boltzmann Equation (LBE) via the Discrete Ordinates method (S_N) requires extensive computational resources for large 3-D neutron and gamma transport applications due to the concurrent discretization of the angular, spatial, and energy domains. This paper will discuss the development RAPTOR-M3G (RApid Parallel Transport Of Radiation – Multiple 3D Geometries), a new 3-D parallel radiation transport code, and its application to the calculation of ex-vessel neutron dosimetry responses in the cavity of a commercial 2-loop Pressurized Water Reactor (PWR). RAPTOR-M3G is based domain decomposition algorithms, where the spatial and angular domains are allocated and processed on multi-processor computer architectures. As compared to traditional single-processor applications, this approach reduces the computational load as well as the memory requirement per processor, yielding an efficient solution methodology for large 3-D problems. Measured neutron dosimetry responses in the reactor cavity air gap will be compared to the RAPTOR-M3G predictions. This paper is organized as follows: Section 1 discusses the RAPTOR-M3G methodology; Section 2 describes the 2-loop PWR model and the numerical results obtained. Section 3 addresses the parallel performance of the code, and Section 4 concludes this paper with final remarks and future work.

1 Methodology

1.1. *Introduction*

The discrete ordinates method (S_N) is a widely used methodology in the nuclear engineering field to obtain a numerical solution of the Linearized Boltzmann Equation for neutron and gamma radiation transport problems [1]. The numerical solution of the S_N equations is achieved through the concurrent discretization of the phase space, i.e., spatial, angular, and energy domains.

The discretization of the phase space leads to a large number of unknowns involved in the solution of the S_N equations; hence the computational requirements, i.e., main memory required and floating point operations per second may grow beyond current computational capabilities of a typical single-processor workstation. For example, the solution of a full 3-D neutron transport problem for a typical 2-loop Pressurized Water Reactor (PWR), characterized by approximately 1.5 million spatial meshes, an S_8 quadrature set, a P_3 expansion of the scattering kernel, and 47-neutron energy groups,

leads to a main memory requirement of approximately 45 GBytes for the whole problem. The significant computational resources required to solve the aforementioned problem, limit the application of single-processor workstations and associated computer codes.

In order to overcome these difficulties, a set of new solution algorithms for the S_N equations are designed to take advantage of multi-processor computing architectures, i.e., distributed memory architectures [2]. In this type of configuration, a number of physically independent workstations are linked together via a fast network connection, establishing what is generally referred to as a cluster computing environment. These computing platforms have found widespread applications in recent years especially in the fields of scientific computing and large scale numerical simulation. However, efficient algorithms need to be devised in order to take full advantage of the cluster environment. One approach to devise a parallel algorithm for the solution of the S_N equations is to use a domain decomposition approach: the angular, spatial, and/or energy domains are partitioned into subsets which can be independently allocated and processed on multi-processor architectures [2]. Currently available 3-D parallel deterministic transport codes include PENTRAN^{TM} [2] and PARTISN [7].

Domain decomposition algorithms are the basis for a newly developed 3-D parallel radiation transport code: RAPTOR-M3G (RApid Parallel Transport Of Radiation – Multiple 3-D Geometries). The computer code is developed in Fortran 90 using the Message Passing Interface (MPI) parallel libraries [3]. The main characteristics of RAPTOR-M3G are summarized as follows:

- Solution of the multi-group S_N equations on 3-D Cartesian, i.e., RAPTOR-XYZ and cylindrical geometries, i.e., RAPTOR-RTZ [4] on non-uniform orthogonal structured meshes.
- Availability of angular, spatial and hybrid angular/spatial domain decomposition algorithms.
- Positive-definite weighted differencing schemes: Zero/Theta Weighted, and Directional Theta Weighted.
- Automatic generation of level-symmetric quadrature sets up to order 20 [5].
- Parallel memory: used to partition the spatial and angular domains on multiple processors, therefore reducing the memory requirements per processor.
- Parallel tasking: concurrent solution of the S_N equations on multiple processors to reduce computational time as compared to single processor technology.
- Parallel I/O: each processor locally accesses its storage devices to reduce I/O time.
- Direct integration with BOT3P [6], an automated mesh generator, and GIP, a multi-group cross sections pre-processor.

1.2. *Solution of the Discrete Ordinates S_N Equations on Parallel Computing Architectures*

This section describes the discretization of the S_N equations and the domain decomposition algorithms developed in RAPTOR-M3G. The spatial and angular discretization, as well as the angular domain decomposition algorithm described herein is specific for the 3D Cartesian XYZ version of the code. The formulation of the S_N equations developed for RAPTOR-RTZ is different from RAPTOR-XYZ due to the presence of the scattering redistribution term.

The phase space of the S_N equations is discretized, i.e., space, angle, energy; hence, the resulting set of linear algebraic equations is suitable for solution on a digital computer. The energy domain is discretized using the multigroup approach into a number of discrete intervals, i.e., g=1…G, starting with the highest energy particles (g=1), and ending with the lowest (g=G). The transport equation in the multigroup approximation is formulated in Eq. (1).

$$\hat{\Omega}\cdot\vec{\nabla}\psi_g(\vec{r},\hat{\Omega})+\sigma_g(\vec{r})\psi_g(\vec{r},\hat{\Omega})=\sum_{g'=1}^{G}\int_{4\pi}d\Omega'\sigma_{gg'}(\vec{r},\hat{\Omega}'\cdot\hat{\Omega})\psi_{g'}(\vec{r},\hat{\Omega}') \\ +\frac{1}{k}\chi_g\sum_{g'=1}^{G}\nu\sigma_{f,g'}(\vec{r})\phi_{g'}(\vec{r})+q_g^e(\vec{r},\hat{\Omega}). \tag{1}$$

The angular domain is discretized by considering a finite set of directions and by applying an appropriate quadrature integration scheme. Each discrete direction can be visualized as a point on the surface of a unit sphere with an associated surface area which mathematically corresponds to the weight of the quadrature scheme. The combination of the discrete directions and the corresponding weights is referred to as quadrature set. In general, quadrature sets must satisfy a number of conditions in order to be accurate and mathematically determined; several approaches have been proposed in the past, e.g., level-symmetric quadrature set (LQn), Legendre polynomial based quadrature sets [8]. The quadrature sets developed in RAPTOR-M3G are based on the LQn method.

The spatial variable can be discretized with several techniques, e.g., finite difference, finite elements. The formulation developed in RAPTOR-M3G is based on the finite difference approach; the spatial domain is partitioned into computational cells, e.g., fine meshes, where the cross sections are assumed constant within each cell. In 3D Carstesian geometry, the angular flux at the cell-center location is evaluated using Eq. (2).

$$\psi_{i,j,k,m,g}=\frac{q_{i,j,k}+\frac{|\mu_m|}{a_{i,j,k,m,g}\Delta x}\psi_{in,x}+\frac{|\eta_m|}{b_{i,j,k,m,g}\Delta y}\psi_{in,y}+\frac{|\xi_m|}{c_{i,j,k,m,g}\Delta z}\psi_{in,z}}{\frac{|\mu_m|}{a_{i,j,k,m,g}\Delta x}+\frac{|\eta_m|}{b_{i,j,k,m,g}\Delta y}+\frac{|\xi_m|}{c_{i,j,k,m,g}\Delta z}+\sigma_{i,j,k}} \tag{2}$$

In Eq. (2), the angle and energy dependence are denoted by the indices *m* and *g*, respectively. The term $q_{i,j,k}$ represents the sum of the scattering, fission and external

sources at cell-center. The weights $a_{i,j,k,m,g}$, $b_{i,j,k,m,g}$, and $c_{i,j,k,m,g}$ are restricted to vary within a range between 0.5 and 1.0; RAPTOR-M3G utilizes the Theta-Weighted (TW), Zero-Weighted (ZW), or the adaptive Directional Theta Weighted (DTW) differencing schemes to calculate the weights during the transport sweep [9].

The S_N equations are solved marching through each direction starting from the boundary of the problem domain; this solution process is also referred to as *transport sweep*. The angular flux defined at center-cell locations is evaluated starting from boundary conditions or from the boundary angular flux previously calculated in adjacent cells. The cell-center angular flux is calculated using Eq. (2). The angular flux exiting the computational cell is calculated using additional relationships referred to as the "*differencing schemes"*.

The transport sweep is performed within an iterative process which is termed *source iteration*, also known as *fixed point iteration,* or *Richardson iteration*. This process is continued until an appropriate convergence criterion is satisfied, i.e., the relative error on the scalar flux in any norm between two iterations is below a certain cutoff value [10]. For radiation shielding calculations this value is generally set to 1.0e-3 or 1.0e-4.

The parallel algorithms developed in RAPTOR-M3G are based on the decomposition of the angular and/or spatial domains on a network of processors. RAPTOR-M3G creates a virtual topology based on a number of processors allocated to the angular and spatial domains, specified as P_a and P_s respectively. The total number of processors required for any decomposition is $P_n = P_a \cdot P_s$. Based on this information, the network of processors is mapped on the spatial and angular domains creating a virtual topology which associates each processor to its local sub-domain.

The angular domain is partitioned on an octant basis, where the processors specified on the angular domain, are sequentially assigned to the local octants. The local number of octants allocated per processor is given by Eq. (3).

$$N_{loct} = \frac{8}{P_a} \tag{3}$$

The transport sweep is locally performed on N_{loct} octants on P_a processors; an MPI communicator for the angular domain is used to synchronize the angular flux among processors and to account for reflective boundary conditions.

The spatial domain is partitioned along the z-axis by sequentially assigning the P_s processors to a number of x-y planes. The total number of fine meshes along the z-axis, i.e., *km*, is partitioned on P_s processors; a mapping array, i.e., *kmloc*, is used to assign the x-y planes to the P_s processors. The number of x-y planes assigned to the P_s processors is arbitrary; however, the condition in Eq. (4) needs to be satisfied in order to define a spatial decomposition that is topologically consistent with the problem geometry.

$$\sum_{i=1}^{P_s} kmloc(i) = km \tag{4}$$

The flexibility to map the processors on the spatial domain to an arbitrary number of x-y planes is dictated by the fact that the number of z-planes may not be exactly divisible by the number of processors on the spatial domain. In this case, a spatial decomposition strategy could not be applied. However, note that an uneven partitioning of the x-y planes on the P_s processors leads to a computational load imbalance of the processors. A hybrid angular/spatial decomposition is the combination of the two algorithms presented above. Section 3 will describe the advantages of using hybrid domain decompositions.

2 Results

2.1 Full 3-D Transport Model of a 2-loop Commercial PWR Reactor

A 3-D transport model of a 2-loop commercial Pressurized Water Reactor (PWR) is presented in this section. The reactor is characterized by a 12 ft core, thermal shield design, and a 3" reactor cavity air gap. The model geometry and the mesh discretization are generated using the BOT3P code, version 5.2. The model extends from 0.0 cm to 245.0 cm along the x-, and y-axis, and from -200.0 cm to 200.0 cm along the z-axis. The model geometry includes a core-water mixture, core shroud, core barrel, thermal shield, Reactor Pressure Vessel (RPV) including stainless-steel liner, and the reflective insulation. The upper and lower internals regions above and below the reactor core are modeled using a steel-water mixture.

A uniform mesh is applied throughout the model; a mesh size of 2.0x2.0x4.0 cm is specified along the x-, y- and z-axes, respectively, yielding a total of 1,464,100 meshes. Figure 1 shows the geometry and material distribution of the 3D model and a 2-D section of the model on the x-y plane at z=0.0 cm.

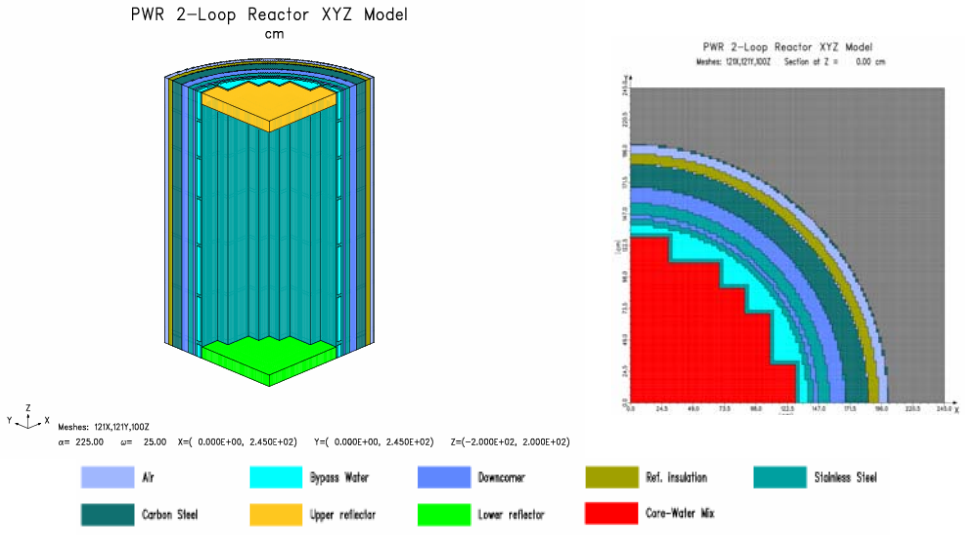

Figure 1. Geometry and material distribution of the 2-loop PWR 3D transport model.

The cross sections for the material mixtures in the transport model are processed using the BUGLE-96 cross sections library [11] and the GIP computer code, part of the DOORS package [12]. An S_8 level symmetric quadrature set and a P_3 spherical harmonics expansion of the scattering kernel is used for the transport calculations.

A system of passive neutron detectors is installed in the reactor cavity air gap between the reflective insulation and the pressure vessel. The dosimetry system provides accurate information relative to the fast neutron exposure over the beltline region of the reactor vessel. Pure metal foils are installed in the reactor cavity, encased in an aluminum shell, which minimizes distortions of the fast neutron spectrum, effectively yielding a free-field measurement. Note that because of this reason, the neutron dosimeters installed in the reactor cavity air gap are not explicitly defined in the transport model. The measured reactions listed in Table 1 are compared with the responses calculated by RAPTOR-M3G.

Table 1. Neutron reactions measured by the dosimetry system.

Material	Reaction
Copper	$^{63}Cu(n,\alpha)^{60}Co$
Iron	$^{54}Fe(n,p)^{54}Mn$
Nickel	$^{58}Ni(n,p)^{58}Co$
Uranium	$^{238}U(n,f)^{137}Cs$
Neptunium	$^{237}Np(n,f)^{137}Cs$

The reactions listed in Table 1 are measured using Cadmium shielded metal foils; therefore, the thermal component of the neutron spectrum is suppressed.

2.2 Comparison of measured dosimetry responses versus RAPTOR-M3G predictions

This section presents the comparison between the measured dosimetry responses and the corresponding predictions obtained with RAPTOR-M3G. The IRDF-2002 dosimetry library [13] is used to generate the calculated dosimetry responses for the neutron reactions listed in Table 1. The measured responses are obtained at four azimuthal locations, i.e., 0˚, 15˚, 30˚, and 45˚, at core mid-plane, in the reactor cavity air gap. Since 2-loop PWR reactors are characterized by peak fast neutron fluence at the 0˚ position, due to close proximity of the nuclear fuel with the RPV, additional measurement are obtained at this location. Specifically at 0˚, measurements are obtained axially at the top and bottom of active core.

Note that initially the calculated dosimetry responses were found to consistently over-predict the measured data. Further investigation revealed that the RPV thickness used in the transport model was smaller than what has been measured during the In-Service Inspection (ISI) of the RPV, confirming our initial findings. The new RPV thickness was introduced into the transport model, and the accuracy of the calculated dosimetry data was improved on the average by ~8%. Figure 2 presents the measured vs.

calculated (M/C) ratios of the dosimetry data calculated using the DTW adaptive differencing scheme.

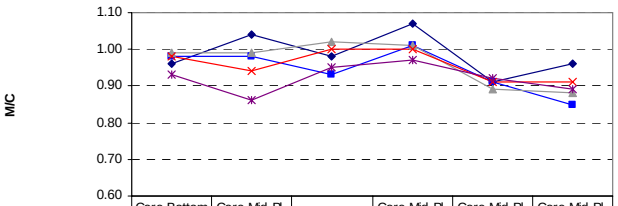

	Core Bottom 0°	Core Mid-Pl. 0°	Core Top 0°	Core Mid-Pl. 15°	Core Mid-Pl. 30°	Core Mid-Pl. 45°
Copper	0.96	1.04	0.98	1.07	0.91	0.96
Iron	0.98	0.98	0.93	1.01	0.91	0.85
Nickel	0.99	0.99	1.02	1.01	0.89	0.88
Uranium	0.98	0.94	1.00	1.00	0.91	0.91
Neptunium	0.93	0.86	0.95	0.97	0.92	0.89

Dosimetry Location

Figure 2. M/C ratios obtained with the DTW adaptive differencing scheme for different materials.

As shown if Figure 2 the M/C ratios are consistently located within a 10% range at each location and for every dosimetry material. The over-prediction at the 30˚ and 45˚ azimuthal positions could be reduced by using a non-uniform mesh refinement at these locations, where the curvature of the system becomes more relevant. The average M/C ratio over all dosimetry locations is 0.96.

Figures 3a through 3c present the M/C values obtained with the ISI-corrected RPV thickness and compare them to the value obtained without the thickness correction. The comparison is presented for all the dosimetry specimens located at the 0˚ azimuthal location.

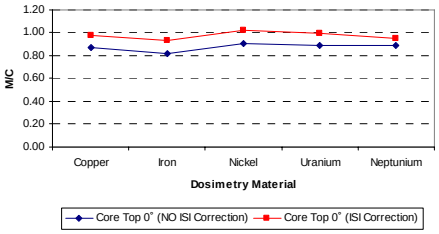

Figure 3a. Comparison of M/C ratios at 0˚ core top location

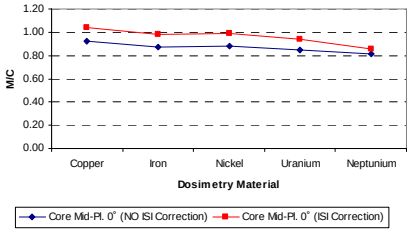

Figure 3b. Comparison of M/C ratios at 0˚ core mid-plane location

Note that the corrected RPV thickness using the ISI measurements improves the accuracy of the calculated responses at every dosimetry location. Similar results are obtained also at 15˚, 30˚, and 45˚ azimuthal locations.

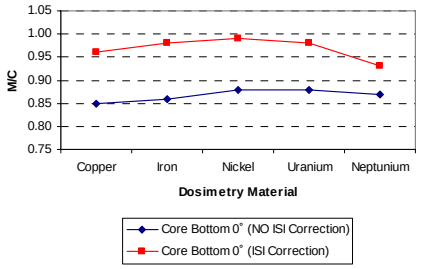

Figure 3c. Comparison of M/C ratios at 0° core bottom location

Table 2. Measured and calculated reactions (DPS/NUCLEUS) rates obtained with the DTW differencing scheme.

	Core Bottom Capsule 0°			Core Mid-Plane Capsule 0°		
Reaction	**Measured**	**Calculated**	**M/C**	**Measured**	**Calculated**	**M/C**
^{63}Cu(n,α)^{60}Co	3.83E-19	4.01E-19	0.96	1.07E-18	1.03E-18	1.04
^{54}Fe(n,p)^{54}Mn	3.60E-17	3.69E-17	0.98	9.41E-17	9.61E-17	0.98
^{58}Ni(n,p)^{58}Co	5.26E-17	5.32E-17	0.99	1.38E-16	1.39E-16	0.99
^{238}U(n,f)^{137}Cs	2.18E-16	2.23E-16	0.98	5.54E-16	5.86E-16	0.94
^{237}Np(n,f)^{137}Cs	3.41E-15	3.67E-15	0.93	8.48E-15	9.85E-15	0.86
	Core Top Capsule 0°			**Core Mid-Plane Capsule 15°**		
Reaction	**Measured**	**Calculated**	**M/C**	**Measured**	**Calculated**	**M/C**
^{63}Cu(n,α)^{60}Co	3.86E-19	3.95E-19	0.98	9.86E-19	9.20E-19	1.07
^{54}Fe(n,p)^{54}Mn	3.37E-17	3.63E-17	0.93	8.45E-17	8.40E-17	1.01
^{58}Ni(n,p)^{58}Co	5.36E-17	5.24E-17	1.02	1.22E-16	1.21E-16	1.01
^{238}U(n,f)^{137}Cs	2.19E-16	2.19E-16	1.00	5.05E-16	5.03E-16	1.00
^{237}Np(n,f)^{137}Cs	3.43E-15	3.62E-15	0.95	8.16E-15	8.42E-15	0.97
	Core Mid-Plane Capsule 30°			**Core Mid-Plane Capsule 45°**		
Reaction	**Measured**	**Calculated**	**M/C**	**Measured**	**Calculated**	**M/C**
^{63}Cu(n,α)^{60}Co	7.45E-19	8.17E-19	0.91	7.15E-19	7.47E-19	0.96
^{54}Fe(n,p)^{54}Mn	6.53E-17	7.15E-17	0.91	5.48E-17	6.44E-17	0.85
^{58}Ni(n,p)^{58}Co	9.04E-17	1.02E-16	0.89	8.08E-17	9.17E-17	0.88
^{238}U(n,f)^{137}Cs	3.72E-16	4.10E-16	0.91	3.29E-16	3.63E-16	0.91
^{237}Np(n,f)^{137}Cs	6.10E-15	6.61E-15	0.92	5.18E-15	5.82E-15	0.89

Table 2 presents the measured and calculated reaction rates at each dosimetry location, as well as the M/C ratio using the RPV thickness corrected with ISI measurements. The average M/C ratio for the reactions listed in Table 2 across all the dosimetry locations is 0.96.

3 RAPTOR-M3G Parallel Performance Analysis

The transport calculations discussed in the previous sections are performed with RAPTOR-M3G running on a 20 processors computer cluster, i.e., EAGLE-1. The cluster is composed of 5 nodes with 2 dual-core dual-processor AMD Opteron 64-bit architecture. The cluster total memory, i.e., RAM, available amounts to 40 GByte; the network interconnection is characterized by 1 GBit/s bandwidth. With this hardware configuration, RAPTOR-M3G completed the full 3D transport calculation for the 2-loop PWR in approximately 106 minutes on 20 processors. No significant differences in performance have been observed using the DTW, TW, or ZW differencing schemes.

Moreover, a simple test problem has been set up to analyze the parallel performance of the code. The test problem consists of 50x50x50 cm box with a uniform distributed fixed source, discretized with a 1 cm uniform mesh. An S_8 quadrature set and P_0 isotropic scattering are used, along with a one energy group cross section set.

The wall-clock time, speed-up, and parallel efficiency are used to evaluate the parallel performance of RAPTOR-M3G. Speed-up and parallel efficiency are defined in Eq. 5 and 6, respectively.

$$S_p = \frac{T_s}{T_p} \tag{5}$$

$$\eta_p = \frac{S_p}{N_p} \tag{6}$$

where, T_s and T_p are the wall-clock times required by the single-processor and multi-processor calculations, respectively. N_p is the number of processors utilized to achieve the wall-clock time T_p. Figure 4 shows a comparison of the speed-up obtained up to 20 processors using different decomposition strategies.

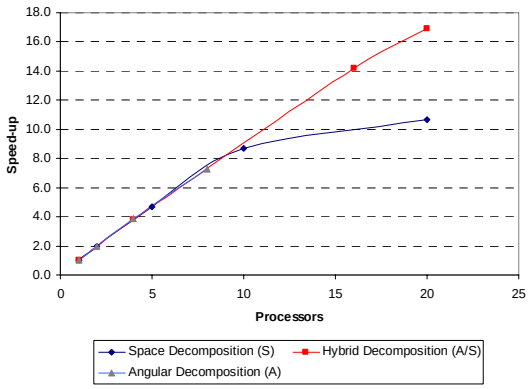

Figure 4. Comparison of RAPTOR-M3G speed-up obtained with different domain decomposition strategies

The speed-up obtained with the space decomposition is progressively reduced as the number of processors is increased. This behavior is due to a finer computational granularity per processor; as the space domain is decomposed into smaller sub-domains, the number of operation per processor is reduced while the inter-processor communication time is increased; therefore leading to a reduced performance. The network data transfer among the nodes is generally the limiting factor on distributed memory architectures. The larger number of iteration required to converge the problem further contributes to reduce the performance of the space decomposition strategy.

However, the hybrid decomposition where the angular and spatial domains are concurrently partitioned yields better results. This behavior is due to the coarser computational granularity induced by this decomposition; also for the hybrid decomposition, the number of iterations required to converge the problem does not increase as much as the space decomposition.

4 Conclusions

A new parallel 3-D radiation transport code has been developed with domain decomposition algorithms, namely RAPTOR-M3G. The code is proven to be accurate and efficient for the solution of radiation transport problems on large and realistic models of commercial nuclear reactors.

Calculated fast neutron reactions in the reactor cavity air gap of a 2-loop PWR agree with measurements on the average by 97%. The solution of the transport problem is obtained in approximately 106 minutes on a 20-processors computer cluster using a hybrid angular/space domain decomposition strategy.

In the future, we are planning to apply the code to typical radiation transport benchmark problems and to more PWR and BWR reactors. Additional research work will also be performed on new iterative schemes to improve on the efficiency of the source iteration method.

References

1. R. Sanchez and N. J. McCormick, "A Review of Neutron Transport Approximations," *Nuclear Science and Engineering*, **Vol. 80**, pp. 481-535 (1982).
2. Sjoden G. E. and Haghighat A., "PENTRAN – Parallel Environment Neutral-particle TRANsport in 3-D Cartesian Geometry," *Proceedings of the Joint International Conference on Mathematical Methods and Supercomputing for Nuclear Applications*, **Vol. 1**, pp. 232-234, Saratoga Springs, NY (1997).
3. Gropp W., Lusk E., and Skjellum A., *Using MPI Portable Parallel Programming with the Message Passing Interface*, The MIT Press, Cambridge, Massachussetts (1999).
4. M. A. Hunter, G. Longoni, and S. L. Anderson, "Extension of RAPTOR-M3G to r-θ-z geometry for use in reactor dosimetry applications," *Proceedings of the 13th International Symposium on Reactor Dosimetry*, The Netherlands (2008).
5. Longoni G. et al., "Investigation of New Quadrature Sets for Discrete Ordinates Method with Application to Non-conventional Problems," *Transactions of the American Nuclear Society*, **Vol. 84**, pp. 224-226 (2001).
6. R. Orsi, "Potential Enhanced Performances in Radiation Transport Analysis on Structured Mesh Grids Made Available by BOT3P," *Nuclear Science and Engineering*, **Vol. 157**, pp. 110-116 (2007).
7. RSICC Computer Code Collection CCC-707, *PARTISN 2.99 : Multi-Dimensional, Time-Independent or Time-Dependent, Multigroup, Discrete Ordinates Transport Code System*.
8. Longoni G. and Haghighat A., "Development of New Quadrature Sets with the Ordinate Splitting Technique," *Proceedings of the ANS International Meeting on Mathematical Methods for Nuclear Applications (M&C 2001)*, Salt Lake City, UT, September 9-13, 2001, American Nuclear Society, Inc., La Grange Park, IL (2001).
9. B. Petrovic and A. Haghighat, "New Directional Theta-Weighted S_N Differencing Scheme and its Application to Pressure Vessel Fluence Calculations," *Proceedings of the 1996 Radiation Protection and Shielding Topical Meeting*, Falmouth, MA, **Vol. 1**, pp. 3-10 (1996).
10. Adams M. L. and Larsen E. W., "Fast Iterative Methods for Discrete-Ordinates Particle Transport Calculations," *Progress in Nuclear Energy*, **Vol. 40**, n. 1 (2002).
11. RSICC Data Library Collection BUGLE-96, "Coupled 47 Neutron, 20 Gamma-Ray Group Cross Section Library Derived from ENDF/B-VI for LWR Shielding and Pressure Vessel Dosimetry Applications," Oak Ridge National Laboratory, Oak Ridge, TN (1999).
12. RSICC Computer Code Collection DOORS 3.2a, "One, Two- and Three Dimensional Discrete Ordinates Neutron/Photon Transport Code System," Oak Ridge National Laboratory, Oak Ridge, TN (2003).
13. I. Kodeli and A. Trkov, "Validation of the IRDF-2002 Dosimetry Library," *Nuclear Instruments and Methods in Physics Research Section A: Accelerators, Spectrometers, Detectors and Associated Equipment*, **Vol. 57, Issue 3**, pp. 664-681 (2007).